Chemistry
A European
Journal

Chemistry Europe
European Chemical Societies Publishing

Accepted Article

Title: Aromaticity Survival in Hydrofullerenes: The Case of C66H4 with its π-Aromatic Circuits

Authors: Dandan Chen, Dariusz W. Szczepanik, Jun Zhu, Alvaro Muñoz-Castro, and Miquel Solà

To be cited as: *Chem. Eur. J.* 10.1002/chem.202004322

Link to VoR: https://doi.org/10.1002/chem.202004322

WILEY-VCH

10.1002/chem.202004322

WILEY-VCH

FULL PAPER

Aromaticity Survival in Hydrofullerenes: The Case of $C_{66}H_4$ with its π-Aromatic Circuits

Dandan Chen,[ab] Dariusz W. Szczepanik,[bc] Jun Zhu,[a] Alvaro Muñoz-Castro*[d] and Miquel Solà*[b]

Dedication ((optional))

[a] Dandan Chen, Prof. Dr. Jun Zhu
State Key Laboratory of Physical Chemistry of Solid Surfaces and Collaborative Innovation Center of Chemistry for Energy Materials (iChEM), Fujian Provincial Key Laboratory of Theoretical and Computational Chemistry and Department of Chemistry, College of Chemistry and Chemical Engineering, Xiamen University, 361005, Xiamen, China.
[b] Dandan Chen, Dr. Dariusz W. Szczepanik and Prof. Dr. Miquel Solà
Institute of Computational Chemistry and Catalysis and Department of Chemistry, University of Girona, C/ M. Aurèlia Capmany, 69, 17003 Girona, Catalonia, Spain.
E-mail: miquel.sola@udg.edu
[c] Dr. Dariusz W. Szczepanik
K. Guminski Department of Theoretical Chemistry, Faculty of Chemistry, Jagiellonian University, Gronostajowa, 2, 30-387 Kraków, Poland.
[d] Dr. Alvaro Muñoz-Castro
Grupo de Química Inorgánica y Materiales Moleculares, Facultad de Ingeniería, Universidad Autónoma de Chile, El Llano Subercaseaux 2801, Santiago, Chile.
E-mail: alvaro.munoz@uautonoma.cl.

Supporting information for this article is given via a link at the end of the document.((Please delete this text if not appropriate))

Abstract: The isolated-pentagon rule (IPR) is a determining structural feature accounting for hollow fullerene stabilization and properties related to C_n ($n \geq 60$) cages. The recent characterization of an unprecedented non-IPR hydrofullerene, C_{2v}-$C_{66}H_4$, bearing two heptagons with adjacent fused-pentagons motif, largely dismiss this feature. Herein, employing DFT calculations, we explore the ^{13}C-NMR pattern and aromatic behavior of C_{2v}-$C_{66}H_4$. Our results show the presence of three π-aromatic circuits at the bottom boat section of $C_{66}H_4$ indicating the unique features of this hydrofullerene in comparison to pristine C_{60}. In addition, under specific orientations of the external field, certain π-aromatic circuits are enabled, resulting in a more aromatic fullerene than C_{60}, but lower in comparison to the spherical aromatic C_{60}^{6-} fulleride. Noteworthy, under a field-aligned along with the saturated carbon atoms, non-aromatic characteristics are exposed. This reveals that spherical-like cages can involve a complex magnetic response that heavily depends on the orientation of the applied field.

Introduction

The unique properties of fullerenes and related species have been of interest since the initial observation of Buckminsterfullerene, C_{60},[1–4] as part of Kroto's research interest in microwave spectroscopy of the outer-space[5] carbon structures. The early characterization of C_{60}[1,2] triggered efforts devoted to understanding the mechanism of synthesis[6] and the relationship between its polyhedral structure and fullerene properties,[7–12] with a wide range of applications from biomedicine to material science.[13–20]

The highly symmetrical C_{60} structure resulting in an aesthetically-pleasing cage involves 12 pentagonal and 20 hexagonal rings obeying the isolated-pentagon rule (IPR)[21–23] that states that the most stable fullerene structures are those that present the 12 pentagons isolated from each other. Species involving modifications of the C_{60} structure are of interest because they inform us how the physicochemical properties change in comparison to the spherical cage of pristine C_{60}. Usually, these modifications result in fused pentagons (non-IPR cages) that can be stabilized either by endohedral metal clusters[24] or by external atoms or groups, as characterized for a series of halogenated fullerenes by Xie and coworkers[25] ($C_{50}Cl_{10}$) among others, with interesting aromatic properties.[26–30]

Recently, Zheng and coworkers characterized the unprecedented formation of a non-IPR hydrofullerene, $C_{66}H_4$, which includes two motifs of a heptagon with two adjacent fused pentagons obtained from low-pressure combustion of a benzene-acetylene-oxygen mixture.[31] $C_{66}H_4$ exhibits a C_{2v}-cage with nineteen unique carbon atoms, which is in contrast to C_{60} displaying the equivalence for all its 60 carbon atoms (*i.e.,* one unique atom type) as indicated by the characteristic single ^{13}C-Nuclear Magnetic Resonance (^{13}C-NMR) resonance pattern observed at 143.15 ppm at room temperature.[32,33]

The spherical structure of C_{60} was coined as the first example of a spherical aromatic molecule[1,11,22] being the prototypical species for this class of compounds.[34–37] However, its aromatic character has been put on controversy[38] due to its local aromatic hexagons and local antiaromatic pentagons rising a non-aromatic character, as a more appropriate definition given by its 60 π-electron system not fulfilling the Hirsch rule.[11,30,39–46] Indeed, C_{60} is considered spherically π-antiaromatic or at least

10.1002/chem.202004322

non-aromatic.[47] However, its hexaanion form, C_{60}^{6-}, is π-aromatic.[42] $\delta(^3He)$ in $^3He@C_{60}^{6-}$ is strongly shifted to higher field[41,48] and $NICS_{total}/NICS_{\pi}$ in the center of the cage diminishes from 0.1/21.2 to -46.2/-24.4 ppm when C_{60} is reduced to C_{60}^{6-}.[42]

Interestingly, the changes introduced in $C_{66}H_4$ may be able to create different aromatic pathways in the roughly spherical cage since the departure from sphericity and inclusion of heptagons[49] modify the behavior of its π-surface. This, in turn, may lead to a diverse pattern of its ^{13}C-NMR *fingerprint*. This provides an interesting case to evaluate how fullerene cages behave when bearing different defects such as heptagons, fused-pentagons, and saturated carbon atoms. The results obtained could be informative towards a concise picture of the structure-property relationship in fullerenes and the related aromatic character, as an extension of the well-discussed aromaticity of IPR fullerenes.

Herein, we explore the characteristics of the π-surface of $C_{66}H_4$ in terms of the different π-circuits along its fullerene cage, by employing density functional theory (DFT) methods to characterize the ^{13}C-NMR pattern owing to the different unique carbon atom types and the resulting local and global magnetic response. In addition, the π-aromatic circuits are scrutinized by the electron density of delocalized bonds (EDDB),[50,51] and gauge-including magnetically induced currents (GIMIC)[52–54] calculations. A recent work[55] has demonstrated that the aromaticity observed in *closo*-boranes and -carboranes is also present in their *nido* "open" counterparts, and consequently, aromaticity in boron clusters survives major structural changes. Following this idea, we aim to analyze whether hydrogenation of fullerenes destroys or (more or less) maintains the aromaticity (understood in terms of electron delocalization and presence of diatropic ring currents) of the fullerenic cage.

Computational Details

Geometry optimizations and subsequent calculations were performed at the DFT level employing the ADF code.[56,57] We used the all-electron triple-ζ Slater basis set augmented with double polarization functions (STO-TZ2P) and the non-local Becke-Perdew (BP86) functional within the generalized gradient approximation (GGA).[58–60] London dispersion corrections to DFT were made using the pairwise method of Grimme (DFT-D3),[61] in addition to the BP86 functional, BP86-D3. The nuclear magnetic shielding tensors were calculated with the NMR module of ADF using gauge-including atomic orbitals (GIAO)[62–65] with the exchange expression proposed by Handy and Cohen,[66] the correlation expression proposed by Perdew, Burke, and Ernzerhof[67] (OPBE), and an all-electron STO-TZ2P basis set. It has been shown that OPBE/TZ2P yields ^{13}C-NMR chemical shifts of similar quality as those provided by CCSD(T)/aug-cc-pVTZ.[68] To account for the ^{13}C-NMR chemical shifts, we used benzene as a secondary reference relative to tetramethylsilane (TMS), according to $\delta^C = \delta^{CBenzene} + \sigma^{CBenzene} - \sigma^C$, where $\delta^{CBenzene} = 128.06$ ppm[69] and $\sigma^{CBenzene} = 64.91$ ppm. This approach agrees well with experimental data as observed in previous studies of fused ring systems,[70] which does not requires further use of scaling factors allowing further direct comparison of the calculated values between different fullerenes and hydrocarbon species. For ^{1}H-NMR $\delta^H = \delta^{HBenzene} + \sigma^{HBenzene} - \sigma^H$, where $\delta^{HBenzene} = 7.16$ ppm[69] and $\sigma^{HBenzene} = 23.75$ ppm. Root-Mean-Square Deviations (RMSD) were obtained by the Chemcraft[71] structural comparison feature. Finally, electron delocalization studies with the EDDB method and magnetically induced currents analysis with GIMIC[53,54,72] have been performed at the CAM-B3LYP/6-311G(d,p)//B3LYP/6-31G(d) level.[73–75] Recent studies shows that long range corrected functionals provide better estimates of electron delocalization than noncorrected exchange-correlation functionals.[76,77] Gaussian 09 software packages[78] and NBO 6.0 program[79] were used in NICS, EDDB, and GIMIC calculations.

Results and Discussion

The characterized $C_{66}H_4$ structure shows two motifs containing a heptagon with two adjacent fused pentagons and four saturated carbon atom in a C_{2v}-cage (Figure 1).[31] The calculated structure is in a good agreement with the experimental one. The geometrical similarity between the two molecular structures is given by the RMSD of 0.04 Å. The calculated ^{1}H-NMR signals at 6.06 and 5.65 ppm are similar to the characterized (6.07 and 5.93 ppm) for both groups of hydrogens,[31] with the H atoms nearby the heptagons located at low-field. The resulting structure exhibits a charge depletion at the region showing the heptagons and fused pentagons motif owing to the saturated character of involved atoms, with an accumulation at the bottom boat shape, as denoted by the electrostatic potential surface (Figure 1b).

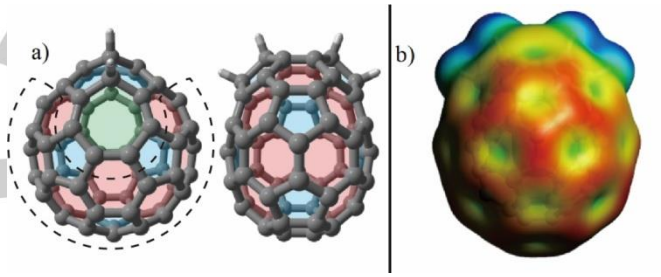

Figure 1. a) Two side-views of $C_{66}H_4$ denoting heptagons (green), hexagons (red), and pentagons (blue). In addition, b) electrostatic potential surface is mapped on isosurfaces of 0.001 a.u. of electron density. The boat region is highlighted with dashed lines. Different views of the electrostatic potential surface are provided in the Supporting Information.

^{13}C-NMR spectra is a valuable technique to obtain relevant information about molecular symmetries and detailed insights into the individual chemical environment from each carbon atom type in fullerenes.[32,33,80–82] Due to its high symmetry, C_{60} exhibits the equivalence of its all 60 atoms denoted by the ^{13}C-NMR single resonance located at 143.15 ppm.[32,33] In contrast, the cage landscape raised by $C_{66}H_4$ results in nineteen unique carbon atom types leading to a more complicated spectrum that has not been discussed in the literature to date. In order to explore the particular ^{13}C-NMR pattern of $C_{66}H_4$, we performed NMR calculation parameters[54,83] showing a pattern of seventeen well-resolved peaks, since two signals are overlapped at ~151.7 ppm (Figure 2). Four sp^2-C atoms from heptagons are located at higher-field (133.5 ppm 129.7 ppm), whereas the sp^2-C atoms bonded directly to the saturated carbon are expected at 153.0 ppm. sp^3-C are expected at 63.3 ppm for carbons closing the heptagon, and at 64.9 ppm for carbons member of the top hexagon. The remaining sp^2-atoms from the top hexagon are calculated at 153.3 ppm. Moreover, the incorporation of the saturated atoms and heptagons results in strong modification of the remaining sp^2-carbons, which ranges from 152 to 140 ppm at the bottom boat

10.1002/chem.202004322

shape. This observation denotes that the upper motif is able to modify the remaining sp^2-carbon network.

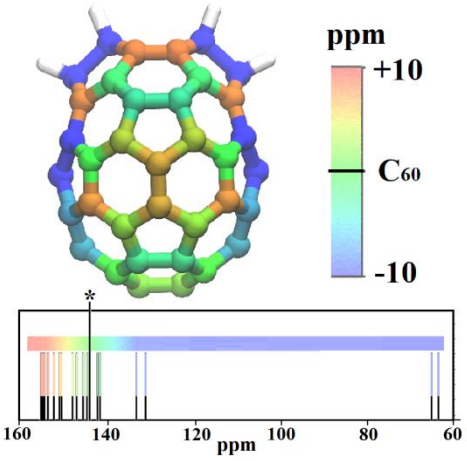

Figure 2. Calculated ^{13}C-NMR spectra for $C_{66}H_4$ in color code ±10 ppm relative to C_{60} (calculated at 142.37 ppm, experimental 143.15 ppm). *denotes calculated ^{13}C-NMR peak for C_{60} (142.37 ppm).

NICS analysis provided by the calculated values at ring centroids allows to evaluate the local aromaticity of individual rings in the fullerene cage, which are also influenced by the fused ring architecture and the upper IPR-violating zone. C_{60} shows paratropicity (anti-aromaticity) and small diatropicity (minor aromaticity), for five- and six-membered rings (5- and 6-MRs), respectively,[44,84–86] with values of 11.8 and -2.4 ppm (NICS(0)$_{iso}$). For C_{60}^{6-}, we observe diatropic ring currents in both rings with negative NICS(0)$_{iso}$ values (-21.9 ppm for the 6-MRs and -21.2 ppm for the 5-MRs).[87,88] Instead of quantifying aromaticity of the rings simply based on NICS values, we focus on the variance of diatropicity and paratropicity of 5-MRs and 6-MRs, which is clearly marked with the out-of-plane index NICS(0)$_{zz}$ (Figure 3). For $C_{66}H_4$, rings consisting of only sp^2 carbons show decreased paratropicity (42.9 to 54.0 ppm for 5-MRs) compared with C_{60} (5-MRs: 61.9 ppm) and mediate diatropicity (-2.0 to 14.9 ppm for 6-MRs) compared with C_{60} (6-MRs: 16.3 ppm) and C_{60}^{6-} (6-MRs: -18.3 ppm). Rings involving sp^3-carbons exhibit values (22.8 to 34.3 ppm) in-between those of 6-MRs (16.3 ppm) and 5-MRs in C_{60} (61.9 ppm). Thus, the capping motif involving heptagons, fused-pentagons and top hexagon range from non-aromatic to antiaromatic regime, with the bottom boat section displaying lesser antiaromatic pentagons and more aromatic hexagons in comparison to C_{60}, suggesting increased aromaticity in the bottom boat section.

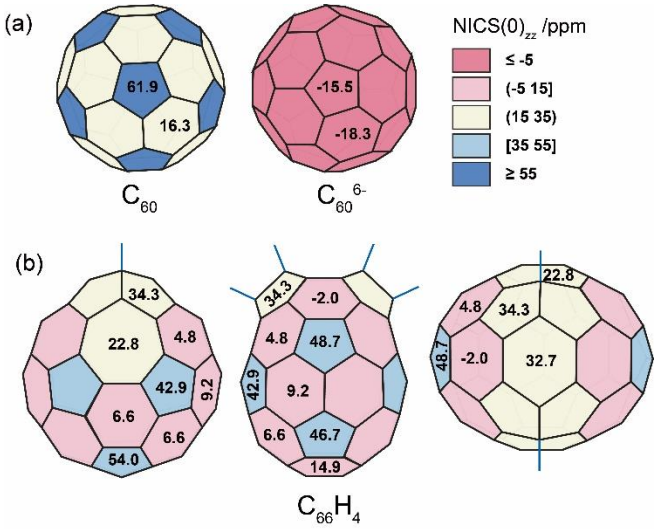

Figure 3. NICS(0)$_{zz}$ values at ring centers for C_{60} and C_{60}^{6-} (a) and $C_{66}H_4$ in three different views (b). Carbon-hydrogen bonds are depicted in blue. Level of theory: B3LYP/6-31G(d). Negative values accounts for regions displaying diatropic currents related to different degrees of aromaticity, whereas positive values accounts for regions compromising paratropic currents related to different degrees of antiaromaticity. The bottom boat region of $C_{66}H_4$ exhibits decreased paratropicity compared with C_{60} while the cap region shows medium paratropicity.

To provide a global picture of the possible enhanced aromatic character of $C_{66}H_4$ in comparison to C_{60} and C_{60}^{6-}, the induced magnetic field (B^{ind})[89,90] was evaluated. The results for $C_{66}H_4$ depicted in Figure 4 shows regions with shielding and deshielding character similar to those found in C_{60} with antiaromatic pentagons and aromatic hexagons. In addition, the top hexagon shows a sizable deshielding region.

Within the magnetic criteria of aromaticity,[91] aromatic species enable a π-electron precession under an external applied magnetic field along with a certain orientation, which in turn builds up an induced magnetic field opposing or shielding the external field, which is useful to rationalize the effect of functional groups or molecules in NMR spectroscopy according to the anisotropy effect.[92–94] For global aromatic species, the π-precession is extended along most of the structural backbones, whereas for local aromatics, this is confined in certain isolated rings.[95] For C_{60}, a short-ranged response is obtained under different orientations of the external field in line to its non-aromatic character (Figure 4).[42] Interestingly, for $C_{66}H_4$ some modifications are observed owing to the enhanced diatropicity (aromaticity) of hexagons leading to a more extended shielding region resulting in an induced shielding cone for two orientations given by B^{ind}_x and B^{ind}_y, which is similar but to a lesser extent to the found for the spherical aromatic C_{60}^{6-} fulleride.[88] However, B^{iso}_z shows a decreased shielding cone shape leading to a similar situation to C_{60}, with a bifurcated complementary deshielding region indicating a non-aromatic behavior under the z-orientation of the applied field.

10.1002/chem.202004322

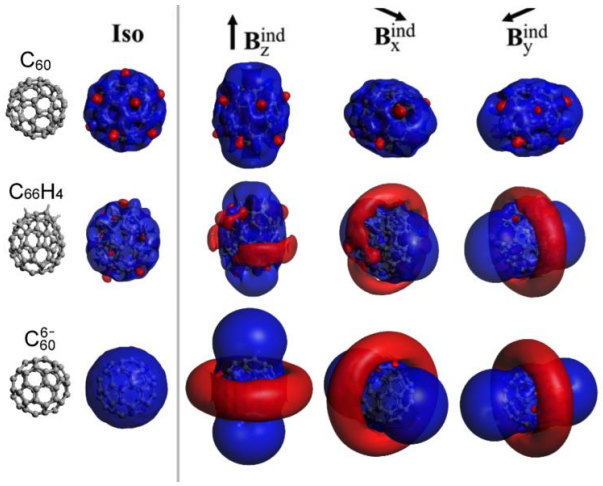

Figure 4. Three-dimensional representations of the induced magnetic field (B^{ind}) accounting for the orientational-averaged (Iso), and specific orientations of the applied field (B^{ind}_i ; *i* = x, y, z) for C_{60}, $C_{66}H_4$, and C_{60}^{6-}. Isosurface set at ±2.0 ppm, Blue: shielding; red, deshielding.

Thus, $C_{66}H_4$ is an interesting case, the first depicted to date, where the low symmetric cage exhibits different aromatic characteristics upon the different orientation of the field, which is introduced by the heptagons/fused-pentagons motif contrasting to C_{60} and other spherical aromatic fullerenes.[88,96] This observation greatly complements the current knowledge on the magnetic behavior in fullerenes, showing that some of them can exhibit a complex pattern dependent on the orientation of the applied field. The origin of this unique pattern for $C_{66}H_4$ is driven by the different π-circuits along the sp^2-backbone located at the bottom boat shape section.

To clarify the possible π-aromatic circuits within the $C_{66}H_4$ structure, the electron density of delocalized bonds (EDDB) method was used,[50] as it provides a uniform approach to quantify and visualize electron delocalization in topologically diversified aromatic systems, and in contrast to the magnetic-response methods, it is derived from the unperturbed 1-electron density. Table 1 includes the maximum, minimum, and average values of atomic contribution and the total values of π-EDDB in the investigated fullerenes C_{60} and $C_{66}H_4$, in addition to C_{60}^{6-} for comparison. It is worth noticing that the population of delocalized π-electrons in C_{60} is almost the same as that in $C_{66}H_4$ despite the different cage characteristics, but sizable lower in comparison to the spherical aromatic C_{60}^{6-} fulleride.

Due to inequivalent ratios of π electrons and carbon atoms, the atomic contributions of π-EDDB are not comparable between these fullerenes. Therefore, we normalized the values using the following equation:

$$EDDB_{norm} = (EDDB/n_{\pi})\times n_{atom} \quad (1)$$

where n_π and n_{atom} are the numbers of π electrons and sp^2 carbon atoms, respectively. The sp^3 carbons of $C_{66}H_4$ are not taken into account, and thus for all neutral systems (C_{60}, and $C_{66}H_4$) the n_π equals the n_{atom}. The normalized atomic contribution of π-EDDB values (Table 2) indicates the most effective electron delocalization in C_{60}^{6-} (0.97e). According to the average values, the magnitude of overall delocalization is the largest in C_{60}^{6-} and smallest in $C_{66}H_4$ ($C_{66}H_4$ < C_{60} < C_{60}^{6-}). However, the lower symmetry of $C_{66}H_4$ (C_{2v}) suggests that the aromatic stabilization effect resides in specific regions (Figure 5).

Table 1. Atomic contribution of π-EDDB for C_{60}, $C_{66}H_4$, and C_{60}^{6-}, and the related normalized atomic contribution of π-EDDB (see text). (Level of theory: CAM-B3LYP/6-311G(d,p)//B3LYP/6-31G(d))

π-EDDB	**C_{60}**	**$C_{66}H_4$**	**C_{60}^{6-}**
Max.	0.80	0.88	1.07
Min.	0.80	0.61	1.07
Avg.	0.80	0.78	1.07
Total	47.89	48.24	64.14
Normalized π-EDDB	**C_{60}**	**$C_{66}H_4$**	**C_{60}^{6-}**
Max.	0.80	0.88	0.97
Min.	0.80	0.61	0.97
Avg.	0.80	0.78	0.97

Figure 5 shows the delocalization patterns by using different colors corresponding to the magnitude of normalized atomic contribution of π-EDDB. Electron delocalization in $C_{66}H_4$ is comparable to C_{60}. In contrast, the hexaanion C_{60}^{6-} features spherical aromatic behavior (despite not following the Hirsch rule,[9] it has a closed t_{1u} subshell electronic structure), in line with the discussed above. Moreover, the sp^3 carbons of $C_{66}H_4$ have a negligible contribution (0.01e) to π electron delocalization in the molecule, and the surrounding area appears to be affected and exhibit weaker delocalization (0.61-0.75e). The remaining part of $C_{66}H_4$ in boat shape (0.80-0.88e) could be considered more aromatic than C_{60}. Therefore, $C_{66}H_4$ could be considered as a partially aromatic fullerene. In fact, $C_{66}H_4$ has two main parts: i) the region containing the heptagon ring together with the C sp^3 atoms can be considered as non-aromatic, and ii) the rest of the fullerenic cage has an aromaticity that is in between that of C_{60} and C_{60}^{6-}.

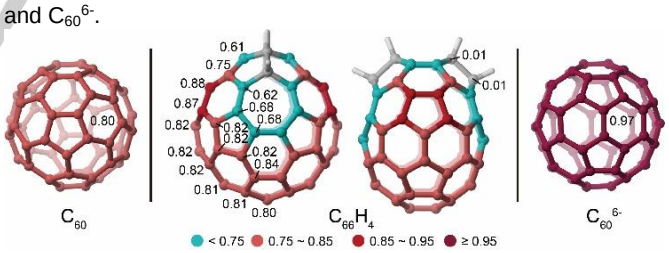

Figure 5. Normalized atomic contribution of π-EDDB for C_{60} (I_h), $C_{66}H_4$ (C_{2v}), and C_{60}^{6-} (I_h). Note, two views of $C_{66}H_4$ are given.

From the π-EDDB isosurfaces (Figure 6), we could confirm that electron delocalization in C_{60}^{6-} is highly efficient, while C_{60} shows weaker delocalization, especially in the outer sphere. Delocalization observed in the outer spheres of $C_{66}H_4$ at the isovalue of 0.015, indicates stronger aromaticity compared with C_{60}, in which isosurface discontinuities are better marked. Based on the larger atomic contribution of π-EDDB values and the more continuous isosurfaces as indicated in Figure 6, we also conclude that in $C_{66}H_4$ the five-membered rings close to the non-aromatic moiety are considerably stabilized by the aromaticity of the bottom boat region. From the analysis of $C_{66}H_4$, we can draw the conclusion that hydrogenation (or more generally functionalization) of fullerenes has an important effect on the local

aromaticity of the hydrogenated C atoms and surroundings but does not make the aromaticity of the rest of the fullerenic cage vanish, even in cases where the IPR rule is not followed. This behavior opposes that of classical planar monocyclic aromatic annulenes for which hydrogenation reduces the aromaticity significantly (although in some cases aromaticity can be partially preserved through homoaromaticity or hyperconjugation).[97–99]

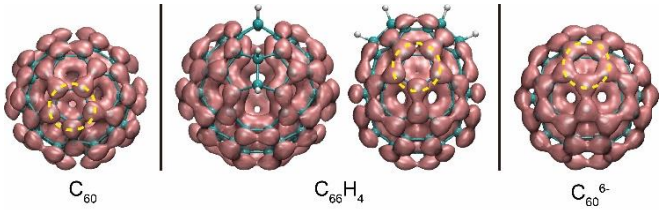

Figure 6. Visualization of π-EDDB with an isovalue of 0.015, for C_{60} (I_h), $C_{66}H_4$ (C_{2v}), and C_{60}^{6-} (I_h). Note, two views of $C_{66}H_4$ are given. The dashed circle highlights the more continuous isosurfaces of a pentagon in $C_{66}H_4$ compared with C_{60}.

Furthermore, three main delocalization π-circuits, or aromatic paths, have been investigated as a source of the aforementioned electron delocalization pathways ascribed to the $C_{66}H_4$ cage (Figure 7). The path 3, following a "naphthalene" circuit has a narrower range of atomic contribution of EDDB (0.28-0.31e). Paths 1 and 2 have a large number of delocalized electrons per C atom, indicating more favorable delocalization pathways, despite having a relatively small value (0.24e) pertaining to the lower 5-MR. Although gauge-including magnetically induced currents (GIMIC) computed for such pathways in $C_{66}H_4$ sustain diatropic induced ring currents observed along the outer perimeters regardless of the direction of $B_0(x,y,z)$ (see supporting information), it is not a straightforward task to determine the aromatic character of $C_{66}H_4$ based only on the GIMIC plots. Interestingly, path 1, which is the one with the highest delocalization, coincides with a path of diatropic circulations in the GIMIC plot.

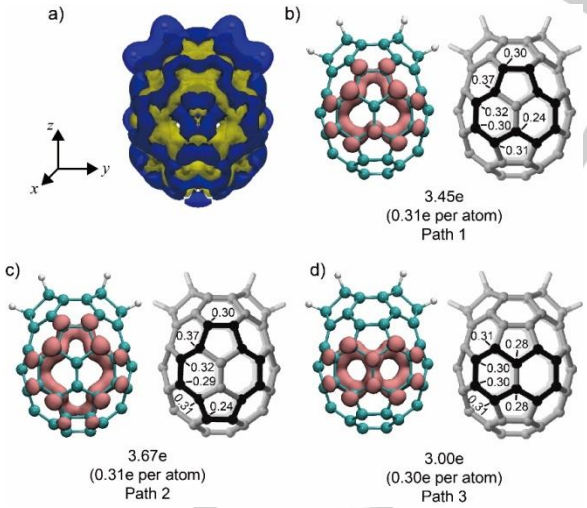

Figure 7. a) Signed modulus density plot of GIMIC and b-d) EDDB results for pathways (in black). Isovalues for GIMIC and EDDB surfaces are 0.02 and 0.01, respectively. The magnetic field is specified along the +*x* direction. Density isosurfaces of GIMIC with diatropic and paratropic contributions are respectively colored blue and yellow. EDDB atomic contributions are presented along the pathways.

Conclusion

$C_{66}H_4$ exhibits unique features in comparison to its parent and highly symmetric I_h-C_{60} owing to the incorporation of two heptagon/fused-pentagon motifs introducing four saturated sp^3-carbon atoms. The remaining sp^2-carbon atoms lead to the formation of three-main π-aromatic circuits ascribed at the bottom boat section of this fullerene derivative. This results in more aromatic features, in comparison to the non-aromatic C_{60}, but decreased in relation to the spherical-aromatic C_{60}^{6-} fulleride, allocating $C_{66}H_4$ as an intermediate case. At variance with planar monocyclic aromatic annulenes, aromaticity in $C_{66}H_4$ does not vanish when one or several C atoms are hydrogenated, although it is almost completely extinguished in the region formed by the sp^3 C atoms and their neighborhood, zone where the IPR rule is broken.

Noteworthy, the lower symmetry and the presence of saturated atoms at the top of the structure results in a unique behavior showing a more aromatic character along two specific orientations of the field aligned along the molecular "equator", but showing non-aromatic characteristics when the field is oriented along with the saturated carbon atoms. This behavior contradicts the spherical aromatic pattern depicted for C_{60}^{6-} for comparison, revealing that spherical-like cages can involve a more complex aromatic character dependent on the orientation of the applied field, which is enabled by the different π-aromatic circuits drawn at the fullerene surface. This shows how the incorporation of different defects in relation to pristine C_{60} modifies the electron delocalization within the fullerene cage. Our results may open new avenues in relation to aromatic fullerenes, where the quest for a dual aromatic/antiaromatic fullerene is on the way.

Acknowledgements

A.M.-C. acknowledges to FONDECYT/ANID 1180683 grant. This work was also supported with funds from the China Scholarship Council (CSC) by a State Scholarship Fund (No. 201906310040, D.C.), the National Science Foundation of China (21873079, J.Z.), the Top-Notch Young Talents Program of China (J.Z.), the Ministerio de Economía y Competitividad (MINECO) of Spain (project CTQ2017-85341-P, M.S.), and the Generalitat de Catalunya (project 2017SGR39, M.S.). D.W.S. acknowledges the financial support by the European Union's Framework Programme for Research and Innovation Horizon 2020 (2014–2020) under the Marie Skłodowska - Curie Grant Agreement No. 797335 "MulArEffect".

Keywords: Fullerenes • Hydrofullerenes • Aromaticity• Defects • Ring currents

References

[1] H. W. Kroto, J. R. Heath, S. C. O'Brien, R. F. Curl, R. E. Smalley, Others, *Nature* **1985**, *318*, 162–163.
[2] R. Taylor, J. P. Hare, A. K. Abdul-Sada, H. W. Kroto, *J. Chem. Soc. Chem. Commun.* **1990**, 1423–1425.
[3] H. W. Kroto, A. W. Allaf, S. P. Balm, *Chem. Rev.* **1991**, *91*, 1213–1235.
[4] W. Krätschmer, K. Fostiropoulos, D. R. Huffman, *Chem. Phys. Lett.* **1990**, *170*, 167–170.
[5] H. Kroto, *Angew. Chem. Int. Ed.* **1997**, *36*, 1578–1593.
[6] D. H. Parker, P. Wurz, K. Chatterjee, K. R. Lykke, J. E. Hunt, M. J.

Pellin, J. C. Hemminger, D. M. Gruen, L. M. Stock, *J. Am. Chem. Soc.* **1991**, *113*, 7499–7503.
[7] W. Wang, J. Dang, X. Zhao, *Phys. Chem. Chem. Phys.* **2011**, *13*, 14629–14635.
[8] P. W. Fowler, T. Heine, *J. Chem. Soc. Perkin Trans. 2* **2001**, 487–490.
[9] A. Hirsch, Z. Chen, H. Jiao, *Angew. Chem. Int. Ed.* **2000**, *39*, 3915–3917.
[10] K. M. Kadish, R. S. Ruoff, *Fullerenes: Chemistry, Physics, and Technology*, John Wiley & Sons Ltd, New York, NY, **2000**.
[11] M. Bühl, A. Hirsch, *Chem. Rev.* **2001**, *101*, 1153–1184.
[12] A. Hirsch, M. Brettreich, *Fullerenes: Chemistry and Reactions*, Wiley-VCH, Weinheim, **2005**.
[13] N. Gharbi, M. Pressac, M. Hadchouel, H. Szwarc, S. R. Wilson, F. Moussa, *Nano Lett.* **2005**, *5*, 2578–2585.
[14] R. Ganesamoorthy, G. Sathiyan, P. Sakthivel, *Sol. Energy Mater. Sol. Cells* **2017**, *161*, 102–148.
[15] Y. Zhang, I. Murtaza, H. Meng, *J. Mater. Chem. C* **2018**, *6*, 3514–3537.
[16] E. Castro, A. H. Garcia, G. Zavala, L. Echegoyen, *J. Mater. Chem. B* **2017**, *5*, 6523–6535.
[17] S. V. Prylutska, A. P. Burlaka, P. P. Klymenko, I. I. Grynyuk, Y. I. Prylutskyy, C. Schütze, U. Ritter, *Cancer Nanotechnol.* **2011**, *2*, 105–110.
[18] A. R. Tuktarov, A. A. Khuzin, N. R. Popod'ko, U. M. Dzhemilev, *Fullerenes, Nanotub. Carbon Nanostructures* **2014**, *22*, 397–403.
[19] J. L. Delgado, P.-A. Bouit, S. Filippone, M. Herranz, N. Martín, *Chem. Commun.* **2010**, *46*, 4853–4865.
[20] M. Izquierdo, B. Platzer, A. J. Stasyuk, O. A. Stasyuk, A. A. Voityuk, S. Cuesta, M. Solà, D. M. Guldi, N. Martín, *Angew. Chem. Int. Ed.* **2019**, *58*, 6932–6937.
[21] R. C. Haddon, L. E. Brus, K. Raghavachari, *Chem. Phys. Lett.* **1986**, *125*, 459–464.
[22] V. Elser, R. C. Haddon, *Nature* **1987**, *325*, 792–794.
[23] H. W. Kroto, *Nature* **1987**, *329*, 529–531.
[24] M. Garcia-Borràs, S. Osuna, M. Swart, J. M. Luis, M. Solà, *Angew. Chem. Int. Ed.* **2013**, *52*, 9275–9278.
[25] S.-Y. Xie, *Science* **2004**, *304*, 699–699.
[26] I. S. Neretin, K. A. Lyssenko, M. Y. Antipin, Y. L. Slovokhotov, O. V. Boltalina, P. A. Troshin, A. Y. Lukonin, L. N. Sidorov, R. Taylor, *Angew. Chem. Int. Ed.* **2000**, *39*, 3273–3276.
[27] A. G. Avent, O. V. Boltalina, J. M. Street, R. Taylor, X.-W. Wei, *J. Chem. Soc. Perkin Trans. 2* **2001**, 994–997.
[28] S. Jenkins, M. I. Heggie, R. Taylor, *J. Chem. Soc. Perkin Trans. 2* **2000**, 2415–2419.
[29] J. Poater, X. Fradera, M. Duran, M. Solà, *Chem. - A Eur. J.* **2003**, *9*, 400–406.
[30] J. Poater, X. Fradera, M. Duran, M. Solà, *Chem. - A Eur. J.* **2003**, *9*, 1113–1122.
[31] H.-R. Tian, M.-M. Chen, K. Wang, Z.-C. Chen, C.-Y. Fu, Q. Zhang, S.-H. Li, S.-L. Deng, Y.-R. Yao, S.-Y. Xie, R.-B. Huang, L.-S. Zheng, *J. Am. Chem. Soc.* **2019**, *141*, 6651–6657.
[32] C. S. Yannoni, R. D. Johnson, G. Meijer, D. S. Bethune, J. R. Salem, *J. Phys. Chem.* **1991**, *95*, 9–10.
[33] R. Tycko, R. C. Haddon, G. Dabbagh, S. H. Glarum, D. C. Douglass, A. M. Mujsce, *J. Phys. Chem.* **1991**, *95*, 518–520.
[34] Z. Chen, R. B. King, *Chem. Rev.* **2005**, *105*, 3613–3642.
[35] P. von R. Schleyer, *Chem. Rev.* **2001**, *101*, 1115–1118.
[36] F. Feixas, E. Matito, J. Poater, M. Solà, *Chem. Soc. Rev.* **2015**, *44*, 6434–6451.
[37] A. I. Boldyrev, L.-S. Wang, *Phys. Chem. Chem. Phys.* **2016**, *18*, 11589–11605.
[38] E. Osawa, H. W. Kroto, P. W. Fowler, E. Wasserman, *Philos. Trans. R. Soc. A Math. Phys. Eng. Sci.* **1993**, *343*, 1–8.
[39] M. Saunders, H. A. Jiménez-Vázquez, R. J. Cross, S. Mroczkowski, D. I. Freedberg, F. A. L. Anet, *Nature* **1994**, *367*, 256–258.
[40] M. Buehl, W. Thiel, H. Jiao, P. v. R. Schleyer, M. Saunders, F. A. L. Anet, *J. Am. Chem. Soc.* **1994**, *116*, 6005–6006.
[41] E. Shabtai, A. Weitz, R. C. Haddon, R. E. Hoffman, M. Rabinovitz, A. Khong, R. J. Cross, M. Saunders, P.-C. Cheng, L. T. Scott, *J. Am. Chem. Soc.* **1998**, *120*, 6389–6393.
[42] Z. Chen, J. I. Wu, C. Corminboeuf, J. Bohmann, X. Lu, A. Hirsch, P. von R. Schleyer, *Phys. Chem. Chem. Phys.* **2012**, *14*, 14886–14891.
[43] D. E. Bean, J. T. Muya, P. W. Fowler, M. T. Nguyen, A. Ceulemans, *Phys. Chem. Chem. Phys.* **2011**, *13*, 20855.
[44] M. P. Johansson, J. Jusélius, D. Sundholm, *Angew. Chem. Int. Ed.* **2005**, *44*, 1843–1846.
[45] J. Poater, M. Duran, M. Solà, *Int. J. Quantum Chem.* **2004**, *98*, 361–366.
[46] M. K. Cyrański, S. T. Howard, M. L. Chodkiewicz, *Chem. Commun.* **2004**, 2458–2459.
[47] M. Garcia-Borràs, S. Osuna, J. M. Luis, M. Swart, M. Solà, *Chem. Soc. Rev.* **2014**, *43*, 5089–5105.
[48] T. Sternfeld, R. E. Hoffman, M. Saunders, R. J. Cross, M. S. Syamala, M. Rabinovitz, *J. Am. Chem. Soc.* **2002**, *124*, 8786–8787.
[49] P. Schwerdtfeger, L. N. Wirz, J. Avery, *Wiley Interdiscip. Rev. Comput. Mol. Sci.* **2015**, *5*, 96–145.
[50] D. W. Szczepanik, M. Andrzejak, J. Dominikowska, B. Pawełek, T. M. Krygowski, H. Szatylowicz, M. Solà, *Phys. Chem. Chem. Phys.* **2017**, *19*, 28970–28981.
[51] D. W. Szczepanik, M. Andrzejak, K. Dyduch, E. Żak, M. Makowski, G. Mazur, J. Mrozek, *Phys. Chem. Chem. Phys.* **2014**, *16*, 20514–20523.
[52] J. Jusélius, D. Sundholm, J. Gauss, *J. Chem. Phys.* **2004**, *121*, 3952–3963.
[53] H. Fliegl, S. Taubert, O. Lehtonen, D. Sundholm, *Phys. Chem. Chem. Phys.* **2011**, *13*, 20500–20518.
[54] D. Sundholm, H. Fliegl, R. J. F. Berger, *Wiley Interdiscip. Rev. Comput. Mol. Sci.* **2016**, *6*, 639–678.
[55] J. Poater, C. Viñas, I. Bennour, S. Escayola, M. Solà, F. Teixidor, *J. Am. Chem. Soc.* **2020**, *142*, 9396–9407.
[56] Amsterdam Density Functional (ADF 2019) Code, Vrije Universiteit: Amsterdam, The Netherlands. Available at: http://www.scm.com
[57] G. Te Velde, F. M. Bickelhaupt, E. J. Baerends, C. Fonseca Guerra, S. J. a. van Gisbergen, J. G. Snijders, T. Ziegler, G. T. E. Velde, C. F. Guerra, S. J. A. Gisbergen, *J. Comput. Chem.* **2001**, *22*, 931–967.
[58] A. D. Becke, *Phys. Rev. A* **1988**, *38*, 3098–3100.
[59] J. P. Perdew, *Phys. Rev. B* **1986**, *33*, 8822.
[60] S. H. Vosko, L. Wilk, M. Nusair, *Can. J. Phys.* **1980**, *58*, 1200–1211.
[61] S. Grimme, *Wiley Interdiscip. Rev. Comput. Mol. Sci.* **2011**, *1*, 211–228.
[62] K. Wolinski, J. F. Hinton, P. Pulay, *J. Am. Chem. Soc.* **1990**, *112*, 8251–8260.
[63] G. Schreckenbach, T. Ziegler, *J. Phys. Chem.* **1995**, *99*, 606–611.
[64] S. K. Wolff, T. Ziegler, E. van Lenthe, E. J. Baerends, *J. Chem. Phys.* **1999**, *110*, 7689.
[65] M. Kaupp, M. Bühl, V. G. Malkin, *Calculation of NMR and EPR Parameters: Theory and Applications*, John Wiley & Sons, Inc., **2006**.
[66] N. C. Handy, A. J. Cohen, *Mol. Phys.* **2001**, *99*, 403–412.
[67] J. P. Perdew, K. Burke, M. Ernzerhof, *Phys. Rev. Lett.* **1996**, *77*, 3865–3868.
[68] L. Armangué, M. Solà, M. Swart, *J. Phys. Chem. A* **2011**, *115*, 1250–1256.
[69] G. R. Fulmer, A. J. M. Miller, N. H. Sherden, H. E. Gottlieb, A. Nudelman, B. M. Stoltz, J. E. Bercaw, K. I. Goldberg, *Organometallics* **2010**, *29*, 2176–2179.
[70] J. Camacho Gonzalez, A. Muñoz-Castro, *Phys. Chem. Chem. Phys.* **2015**, *17*, 17023–17026.
[71] Zhurko, G.A. and Zhurko, D.A. Chemcraft. Version 1.7 (Build 132). http://www.chemcraftprog.com**.**
[72] S. Taubert, D. Sundholm, J. Jusélius, W. Klopper, H. Fliegl, *J. Phys. Chem. A* **2008**, *112*, 13584–13592.
[73] T. Yanai, D. P. Tew, N. C. Handy, *Chem. Phys. Lett.* **2004**, *393*, 51–57.
[74] A. D. Becke, *J. Chem. Phys.* **1993**, *98*, 5648.
[75] C. Lee, W. Yang, R. G. Parr, *Phys. Rev. B* **1988**, *37*, 785–789.
[76] D. W. Szczepanik, M. Solà, M. Andrzejak, B. Pawełek, J. Dominikowska, M. Kukułka, K. Dyduch, T. M. Krygowski, H. Szatylowicz, *J. Comput. Chem.* **2017**, *38*, 1640–1654.
[77] I. Casademont-Reig, T. Woller, J. Contreras-García, M. Alonso, M. Torrent-Sucarrat, E. Matito, *Phys. Chem. Chem. Phys.* **2018**, *20*, 2787–2796.
[78] Gaussian 09, Revision A.02, M. J. Frisch, G. W. Trucks, H. B. Schlegel, G. E. Scuseria, M. A. Robb, J. R. Cheeseman, G. Scalmani, V. Barone, G. A. Petersson, H. Nakatsuji, X. Li, M. Caricato, A. Marenich, J. Bloino, B. G. Janesko, R. Gomperts, B. Mennucci, H. P. Hratchian, J. V. Ortiz, A. F. Izmaylov, J. L. Sonnenberg, D. Williams-Young, F. Ding, F. Lipparini, F. Egidi, J. Goings, B. Peng, A. Petrone, T. Henderson, D. Ranasinghe, V. G. Zakrzewski, J. Gao, N. Rega, G. Zheng, W. Liang, M. Hada, M. Ehara, K. Toyota, R. Fukuda, J. Hasegawa, M. Ishida, T. Nakajima, Y. Honda, O. Kitao, H. Nakai, T. Vreven, K. Throssell, J. A. Montgomery, Jr., J. E. Peralta, F. Ogliaro, M. Bearpark, J. J. Heyd, E. Brothers, K. N. Kudin, V. N. Staroverov, T. Keith, R. Kobayashi, J. Normand, K. Raghavachari, A. Rendell, J. C. Burant, S. S. Iyengar, J. Tomasi, M. Cossi, J. M. Millam, M. Klene, C. Adamo, R. Cammi, J. W. Ochterski, R. L. Martin, K. Morokuma, O. Farkas, J. B. Foresman, and D. J. Fox, Gaussian, Inc., Wallingford CT, 2016.
[79] NBO 6.0. E. D. Glendening, J. K. Badenhoop, A. E. Reed, J. E. Carpenter, J. A. Bohmann, C. M. Morales, C. R. Landis, and F. Weinhold, Theoretical Chemistry Institute, University of Wisconsin, Madison (2013).
[80] J. Kaminský, M. Buděšínský, S. Taubert, P. Bouř, M. Straka, *Phys. Chem. Chem. Phys.* **2013**, *15*, 9223.
[81] C. Piskoti, J. Yarger, A. Zettl, *Nature* **1998**, *393*, 771–774.
[82] T. Heine, M. Bühl, P. W. Fowler, G. Seifert, *Chem. Phys. Lett.* **2000**, *316*, 373–380.
[83] M. Kaupp, in *Calc. NMR EPR Parameters*, Wiley-VCH Verlag GmbH {&} Co. KGaA, Weinheim, FRG, **2004**, pp. 293–306.

[84] A. Pasquarello, M. Schluter, R. C. Haddon, *Science* **1992**, *257*, 1660–1661.
[85] A. Pasquarello, M. Schlüter, R. C. Haddon, *Phys. Rev. A* **1993**, *47*, 1783–1789.
[86] R. Zanasi, P. W. Fowler, *Chem. Phys. Lett.* **1995**, *238*, 270–280.
[87] T. Sternfeld, C. Thilgen, R. E. Hoffman, M. del Rosario Colorado Heras, F. Diederich, F. Wudl, L. T. Scott, J. Mack, M. Rabinovitz, *J. Am. Chem. Soc.* **2002**, *124*, 5734–5738.
[88] N. D. Charistos, A. Muñoz-Castro, *J. Phys. Chem. C* **2018**, *122*, 9688–9698.
[89] R. Islas, T. Heine, G. Merino, *Acc. Chem. Res.* **2012**, *45*, 215–228.
[90] G. Merino, T. Heine, G. Seifert, *Chem. - A Eur. J.* **2004**, *10*, 4367–4371.
[91] R. Gershoni-Poranne, A. Stanger, *Chem. Soc. Rev.* **2015**, *44*, 6597–6615.
[92] M. Baranac-Stojanović, M. Stojanović, *Chem. - A Eur. J.* **2013**, *19*, 4249–4254.
[93] M. Baranac-Stojanović, *RSC Adv.* **2014**, *4*, 308–321.
[94] I. G. Cuesta, A. S. De Merás, S. Pelloni, P. Lazzeretti, *J. Comput. Chem.* **2009**, *30*, 551–564.
[95] A. Muñoz-Castro, *Phys. Chem. Chem. Phys.* **2018**, *20*, 3433–3437.
[96] A. Muñoz-Castro, *Phys. Chem. Chem. Phys.* **2017**, *19*, 12633–12636.
[97] R. V. Williams, *Chem. Rev.* **2001**, *101*, 1185–1204.
[98] D. Chen, Q. Xie, J. Zhu, *Acc. Chem. Res.* **2019**, *52*, 1449–1460.
[99] K. Xiao, Y. Zhao, J. Zhu, L. Zhao, *Nat. Commun.* **2019**, *10*, 5639.

10.1002/chem.202004322

Entry for the Table of Contents

Insert graphic for Table of Contents here. ((Please ensure your graphic is in **one** of following formats))

Insert text for Table of Contents here.

Unique aromatic features of $C_{66}H_4$ are found in comparison to pristine C_{60}, where three π-aromatic circuits are present at the bottom boat section of this fullerene derivative.

Institute and/or researcher Twitter usernames: @amclab @miquelsola @dimocat_iqcc @iqccUdG